Heliyon

Received:
3 October 2017
Revised:
11 January 2018
Accepted:
26 November 2018

Cite as: Daniel Stocker, Herman P. Marquez, Matthias W. Wagner, Dimitri A. Raptis, Pierre-Alain Clavien, Andreas Boss, Michael A. Fischer, Moritz C. Wurnig. MRI texture analysis for differentiation of malignant and benign hepatocellular tumors in the non-cirrhotic liver.
Heliyon 4 (2018) e00987.
doi: 10.1016/j.heliyon.2018.e00987

MRI texture analysis for differentiation of malignant and benign hepatocellular tumors in the non-cirrhotic liver

Daniel Stocker [a,*], **Herman P. Marquez** [b], **Matthias W. Wagner** [a], **Dimitri A. Raptis** [c], **Pierre-Alain Clavien** [c], **Andreas Boss** [a], **Michael A. Fischer** [d], **Moritz C. Wurnig** [a]

[a] *Institute of Interventional and Diagnostic Radiology, University Hospital Zurich and University of Zurich, Zurich, Switzerland*

[b] *Department of Radiology, Hospital Universitario de Canarias, Santa Cruz de Tenerife, Spain*

[c] *Department of Visceral and Transplant Surgery, Swiss Hepato-Pancreato-Biliary (HPB) Center, University Hospital Zurich and University of Zurich, Zurich, Switzerland*

[d] *Department of Radiology, Orthopedic University Hospital Balgrist, University of Zurich, Zurich, Switzerland*

[*] Corresponding author.

E-mail address: daniel.stocker@usz.ch (D. Stocker).

Abstract

Purpose: To find potentially diagnostic texture analysis (TA) features and to evaluate the diagnostic accuracy of two-dimensional (2D) magnetic resonance (MR) TA for differentiation between hepatocellular carcinoma (HCC) and benign hepatocellular tumors in the non-cirrhotic liver in an exploratory MR-study.

Materials and methods: 108 non-cirrhotic patients (62 female; 41.5 ± 18.3 years) undergoing preoperative contrast-enhanced MRI were retrospectively included in this multi-center-study. TA including gray-level histogram, co-occurrence and run-length matrix features (total 19 features) was performed by two independent readers. Native fat-saturated-T1w and T2w as well as arterial and portal-venous post contrast-enhanced 2D-image-slices were assessed. Conventional reading was performed by two separate independent readers. Differences in TA features between HCC and benign lesions were investigated using independent sample

https://doi.org/10.1016/j.heliyon.2018.e00987

t-tests. Logistic regression analysis was performed to obtain the optimal number/combination of TA-features and diagnostic accuracy of TA analysis. Sensitivity and specificity of the better performing radiologist were compared to TA analysis.
Results: The highest number of significantly differing TA-features ($n = 5$) was found using the arterial-phase images including one gray-level histogram (skewness, $p = 0.018$) and four run-length matrix features (all, $p < 0.02$). The optimal binary logistic regression model for TA-features of the arterial-phase images contained 13 parameters with an accuracy of 84.5% (sensitivity 84.1%, specificity 84.9%) and area-under-the-curve of 0.92 (95%-confidence-interval 0.85−0.98) for diagnosis of HCC. Conventional reading yielded a significantly lower sensitivity (63.6%, $p = 0.027$) and no significant difference in specificity (94.6%, $p = 0.289$) at best.
Conclusion: 2D-TA of MR images is a feasible objective method that may help to distinguish HCC from benign hepatocellular tumors in the non-cirrhotic liver. Most promising results were found in TA features in the arterial phase images.

Keywords: Health profession, Medical imaging, Medicine

1. Introduction

Hepatocellular carcinoma (HCC) is the sixth most common cancer, the most common primary malignant liver tumor and in men the second leading cause of death due to cancer worldwide [1]. While HCC most frequently arises in a cirrhotic liver [2], depending on the population, about 7.2−42.6% of HCCs also arise in non-cirrhotic livers [3, 4, 5, 6]. Due to its high overall diagnostic accuracy for focal liver lesions, contrast-enhanced magnetic resonance (MR) imaging is currently the modality of choice for distinction of HCC and benign liver lesions in cirrhotic and non-cirrhotic livers [7, 8]. However, differentiation of HCC from focal nodular hyperplasia (FNH) and hepatic adenoma (HA) with atypical appearance is not always possible in the non-cirrhotic liver using state-of the art non-invasive or invasive techniques [9, 10].

Although most HCCs can be detected by MRI there is limited diagnostic accuracy for atypical lesions in the non-cirrhotic liver, even with hepatocyte-specific contrast media as all hepatocellular tumors might lack or show hepatocyte-specific contrast media uptake [11, 12].

Biopsy is performed in those cases to obtain histopathological diagnosis [13] although it is known that a liver biopsy is limited by a sampling error and high interreader variability, possibly leading to a false diagnosis due to tumor heterogeneity [14, 15]. Moreover, liver biopsy has the potential risk of tumor cell dissemination and intervention related complications like bleeding or infection. However, reliable

https://doi.org/10.1016/j.heliyon.2018.e00987

biomarkers are needed to obtain an early diagnosis as the outcome for patients depends on the grade of HCC dedifferentiation [16, 17].

Texture analysis (TA) is an objective region-of-interest (ROI) based image processing method, which allows to evaluate gray-level image features without the limitations of subjective judgment of a reader [18, 19]. Using TA, the structure of the analyzed image is assessed on several levels, e.g. its distribution of gray-levels in general or in neighboring voxels, and objective measures are derived. In recent years various studies have implemented TA of two-dimensional (2D) MR-images in different parts of the body such as brain [20], prostate [21], breast [22] and liver [23]. In these studies TA proofed to be a promising technique to distinguish or classify benign and malignant lesions [20, 21, 22, 23].

The purpose of our study was to find potentially diagnostic TA features and to evaluate the diagnostic accuracy of 2D-MR-TA for differentiation between HCC and benign hepatocellular tumors in the non-cirrhotic liver in an MR-study.

2. Materials and methods

This study included data from an internationally registered multi-center study (ClinicalTrials.gov: NCT01234701). Institutional review board approval was obtained at the Ethics committee of the Canton Zurich and a waiver of written informed consent was obtained in each site. Data of this study population or parts of it were previously reported in different contexts [24, 25].

2.1. Study population

A total of 108 non-cirrhotic patients (group: median age 45, range 18−85; females (n = 62): 37.5, 18−85; males (n = 46): 55.5, range 24−81) were retrospectively included in this multi-center study of five large international cancer care centers between January 2006 and June 2010. All patients underwent liver resection due to HCC, HA or FNH. Inclusion criteria were 1) age over 18 years, 2) no contraindications for MR-scanning, 3) contrast-enhanced MRI within two months prior to surgery 4) partial liver resection, 5) histopathological diagnosis of HCC, HA or FNH based on the total resected specimen, and 6) histopathological evidence of non-cirrhotic liver-structure surrounding the lesion. Final diagnosis of the tumor was based on histopathology of the largest liver lesion of each patient.

2.2. Histopathological analysis

Macroscopic analysis, tissue sampling of the lesion and the surrounding liver parenchyma as well as an immunohistochemistry analysis was performed in all specimens by the local pathologist at each of the five centers according to local protocols. In

https://doi.org/10.1016/j.heliyon.2018.e00987

patients with more than one liver lesion a radiologist, who was not involved in the image analysis, marked the resected lesion by slice position and location according to the hepatic segment numbering system of Couinaud.

2.3. Magnetic resonance imaging

Image acquisition was performed on 1.5T MRI-scanners (1xGenesis Signa, 1xSigna Horizon, GE Healthcare, Waukesha, WI; 1xSonata, 2xAvanto, Siemens Healthcare, Erlangen, Germany). For MR-imaging local optimized clinical protocols were used. All MRI-protocols comprised of a spin-echo T2-weighted (T2w) sequence and a native fat-saturated gradient-echo T1-weighted (fs-T1w) sequence. Contrast-enhanced fat-saturated gradient-echo T1-weighted sequences according to local optimized MRI-liver-protocols were obtained using an extracellular-fluid agent, a hepatobiliary-specific agent or extracellular-fluid agent in combination with a reticuloendothelial-specific agent. Gadoterate meglumine (Dotarem®, Guerbet AG, Zurich, Switzerland), gadoteridol (ProHance®, Bracco, Milan, Italy) and gadobutrol (Gadovist®, Bayer Schering Pharma AG, Leverkusen, Germany) were used as extracellular-fluid agents, gadoxetic acid (Primovist®, Bayer AG, Leverkusen, Germany) and gadobenate dimeglumine (MultiHance®, Bracco, Milan, Italy) as hepatobiliary-specific agent and ferucarbotran (Resovist®, Bayer Schering Pharma AG, Leverkusen, Germany) at doses as specified by the manufacturer. All protocols included acquisition of an arterial phase (10 seconds after contrast application) and a portal-venous phase (60 seconds after contrast application). In all patients, who received the hepatobiliary-specific agent a hepatospecific phase was acquired (10−30 minutes after contrast application). Relevant acquisition parameters can be found in Table 1.

2.4. Image analysis

2D-TA was implemented in Matlab (MathWorks, Natick, MA) based on work of Vallieres et al. [26] and Wei [27]. In short, gray-levels in the placed ROI were first normalized. Then the first-level TA-features based on the histogram of all gray-levels in the ROI were computed (variance, skewness, kurtosis, entropy). Subsequently, the gray-level co-occurrence matrix (GLCM) was constructed based on the gray-level distribution within the ROI as introduced by Haralick et al [28]. Briefly, this matrix contains the distribution of all possible pairs of gray-levels in neighboring pixels of a given image. Using the GLCM the second-level TA-features contrast, correlation, energy and homogeneity were derived. Finally, the gray-level run-length matrix (GLRLM) was constructed. This matrix basically depicts the distribution of the number of neighboring pixels with the same gray-levels on a straight line in a given image. From the GLRLM the second-level TA-features short-run emphasis (SRE), long-run emphasis (LRE), gray-level nonuniformity (GLN),

https://doi.org/10.1016/j.heliyon.2018.e00987

Table 1. Important MR sequence parameters. T1-weighted native and contrast-enhanced as well as T2-weighted images were used for texture analysis and for conventional reading. Additionally, in- and opposed-phase gradient-echo sequences were analyzed for conventional reading. In institution 1 after application of extracellular contrast medium a reticuloendothelial-specific contrast agent ferucarbotran (0.5 mmol Fe/ml) was additionally applied. None of the sequences with reticuloendothelial-specific contrast agent were used for texture analysis or conventional reading.

Institution	Sequence	Acquisition parameter						Contrast agent	
		Orientation	Matrix	ST [mm]	TR [ms]	TE [ms]	FA [°]	Extracellular	hepatocytespedific
1	T2 FS RT	Axial	256 × 196	5	9474	105	90	Gadoterate meglumine (0.5 mmol Gd/ml)	Gadoxetic acid (0.25 mmol Gd/ml)
	T1 LAVA native	Axial	256 × 224	4	3	1.4	15		
	T1 LAVA dynamic	Axial	256 × 224	4	3	1.4	15		
	T1 in/opp	Axial	224 × 192	5	135	2.2/4.7	60		
2	T2 HASTE fat sat	Axial	256 × 218	4	1100	87	150	Gadoterate meglumine (0.5 mmol Gd/ml)	
	T1 VIBE 3D native	Axial	512 × 176	3	3.5	1.6	12		
	T1 VIBE 3D dynamic	Axial	512 × 176	3	3.5	1.6	12		
	T1 FLASH in/out	Axial	256 × 158	7	120	2.4/4.8	70		
3	T2 FRFSE	Axial	256 × 160	8	2500	91	90	Gadoteridol (0.5 mmol Gd/ml)	Gadobenate dimeglumine (0.5 mmol Gd/ml)
	T1 native	Axial	256 × 192	6	4.3	1.9	15		
	T1 FS dynamic	Axial	256 × 192	6	4.3	1.9	15		
	T1 in/opp	Axial	256 × 160	10	180	2.2/4.7	85		

(*continued on next page*)

https://doi.org/10.1016/j.heliyon.2018.e00987

Table 1. (*Continued*)

Institution	Sequence	Acquisition parameter						Contrast agent	
		Orientation	Matrix	ST [mm]	TR [ms]	TE [ms]	FA [°]	Extracellular	hepatocytespedific
4	T2 HASTE	Axial	256 × 205	5	1000	62	150	Gadoteridol (0.5 mmol Gd/ml)	Gadobenate dimeglumine (0.5 mmol Gd/ml)
	T1 VIBE 3D native	Axial	320 × 166	3	5.2	2.4	10		
	T1 VIBE 3D dynamic	Axial	320 × 166	3	5.2	2.4	10		
	T1 FLASH in/opp	Axial	256 × 208	8	94	2.2/4.9	70		
5	T2 HASTE	Axial	320 × 218	5	1200	66	180	Gadobutrol (1 mmol Gd/ml)	Gadoxetic acid (0.25 mmol Gd/ml)
	T1 VIBE 3D native	Axial	320 × 189	3.5	4.8	2.1	13		
	T1 VIBE 3D dynamic	Axial	320 × 189	3.5	4.8	2.1	13		

Abbreviations: slice thickness (ST); repetition time (TR); echo time (TE); flip angle (FA); T1-weighted imaging (T1); T2-weighted imaging (T2); fat saturated (FS); respiratory trigger (RT); liver acquisition with volume acceleration (LAVA); half Fourier acquisition single shot turbo spin echo (HASTE); volume interpolated breath hold examination (VIBE); fast relaxation fast spin echo (FRFSE); fast low angle shot (FLASH); in-phase and opposed-phase imaging (in/opp).

https://doi.org/10.1016/j.heliyon.2018.e00987

Article No~e00987

run-length nonuniformity (RLN), run percentage (RP), low gray-level run emphasis (LGRE), high gray-level run emphasis (HGRE), short-run low gray-level emphasis (SRLGE), short-run high gray-level emphasis (SRHGE), long-run low gray-level emphasis (LRLGE), and long-run high gray-level emphasis (LRHGE) were obtained. Principles of generating GLCM and GLRLM are summarized in Fig. 1. To minimize the possible impact of the needed choice of a direction for the construction of GLCM and GLRLM second-level TA-features were calculated for all four possible directions and mean values were used for further investigations. Images with severe artefacts resulting in non-definable or only partial definable, not allowing classifying the lesion, were excluded.

For the actual 2D-TA two readers (TA Readers 1 and 2: DS and HM, 2 and 5 years experience in abdominal imaging), blinded to the pathologic diagnostic results as well as the results of each other, independently selected the slice containing the largest diameter of the largest liver lesion in the acquired T2w and native fs-T1w images, the arterial phase, portal-venous phase and if available hepatobiliary phase

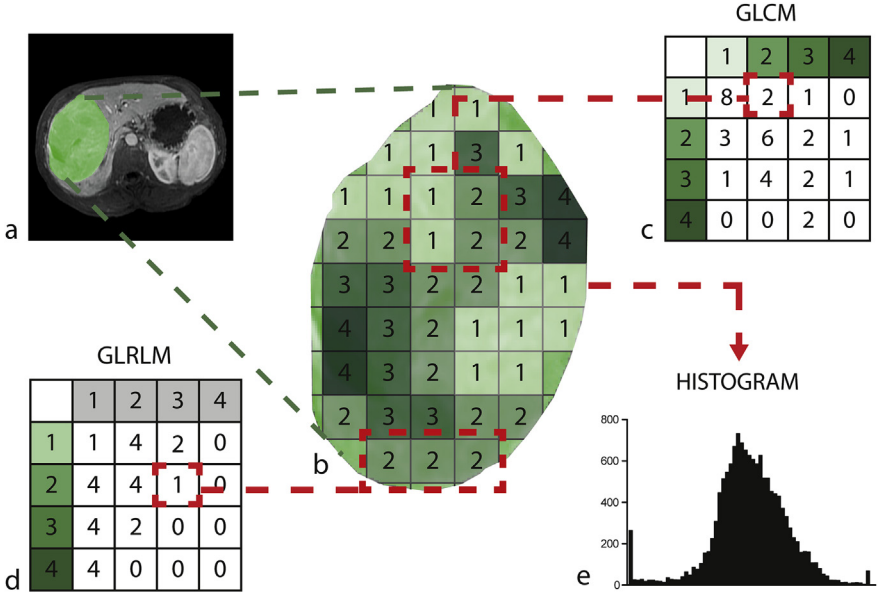

Fig. 1. Schematic overview of the texture analysis process. First, a ROI has to be drawn covering the assessed lesion (a) (green overlay in the upper left). For demonstration purposes projected in the middle of the image with arbitrarily selected and arranged fictive pixels with different gray-levels numbered from one to four as an example (b). From the matrix of values within the ROI a GLCM* (c), a GLRLM* (d) and a histogram (e) is computed. For the GLCM each pixel of the image is scanned and used as a "reference pixel" once. This pixel is then compared with the pixel in a given distance and direction (0°, 45°, 90° or 135°), the "neighbour pixel". When a reference value and a neighbour value pair are found, the GLCM is increased by 1 in the respective column and row (in the example above two pairs of 1:2 are found and a 2 is added in the matrix accordingly). GLRLM quantifies runs of the same gray-level in a given direction (0°, 45°, 90° or 135°). Different to the GLCM the GLRLM has run lengths plotted on the y-axis. The example above shows a run of three 2s and a 1 is added in the matrix accordingly. *for the shown example, a distance of 1 and a direction of 0° was used.

https://doi.org/10.1016/j.heliyon.2018.e00987

images. Subsequently a ROI was defined in this slice including the whole lesion (cp. Fig. 2) and the 19 TA-features described above were calculated.

Additionally, the same sequences, as well as, if available, supplementary in- and opposed-phase gradient-echo sequences were read by two board-certified radiologists blinded to all clinical findings (MR Readers 1 and 2: not authors of the manuscript, 11 and 13 years experience in abdominal imaging). Each lesion was diagnosed as HCC, HA, FNH or cyst, based on the readers personal experience, by applying commonly used MRI-criteria such as contrast enhancement in the arterial phase, contrast media wash-out in the portal venous phase, hyper-enhancement of the capsule in the portal venous phase and vessel invasion. Based on this diagnose the results of both MR readers were classified as either benign or malignant for further analysis.

2.5. Statistical analysis

Interreader agreement for all TA-features and MR-sequences was assessed using the intra-class correlation coefficient (ICC), interreader agreement for conventional reading was measured using Cohen's kappa. An ICC of 0.75−1.00 indicated excellent, 0.60−0.74 good, 0.40−0.59 fair and <0.4 poor agreement. A kappa of 0.81−1.00 indicated very good, 0.61−0.80 good, 0.41−0.60 moderate, 0.21−0.40 fair and <0.20 poor agreement. Independent Student-t-tests were used to detect significant differences in TA-features between HCCs and benign liver lesions. Furthermore, a logistic regression analysis was performed to evaluate the optimal number and combination of TA-features along with the achieved diagnostic accuracy for each MRI-sequence separately. The receiver-operating-characteristic (ROC) curves for the final models were constructed and the respective area-under-the-curve (AUC) as well as their 95% confidence intervals computed. Sensitivity and specificity

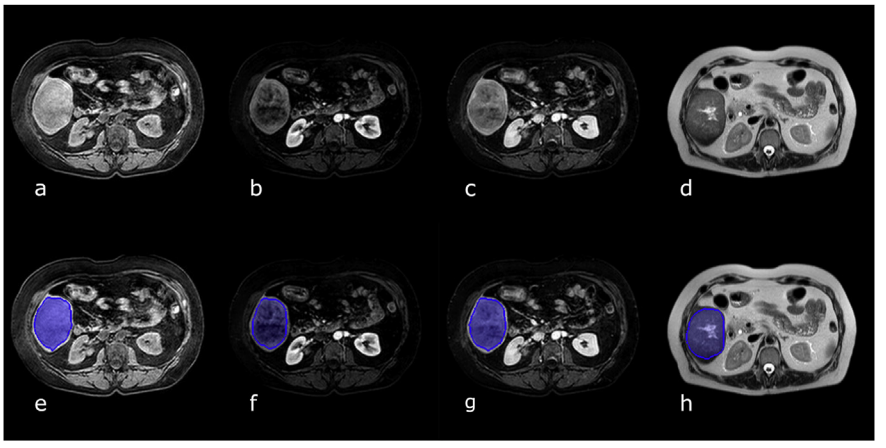

Fig. 2. Typical placement of ROIs in axial MR-images, containing the largest diameter of the lesion. Upper row: native fs-T1w image (a), arterial phase (b), portal-venous phase (c) and T2w image (d). Lower row: manual drawn ROIs covering the whole lesion in blue, native fs-T1w image (e), arterial phase (f), portal-venous phase (g) and T2w image (h).

https://doi.org/10.1016/j.heliyon.2018.e00987

between best performing binary logistic regression model and better performing radiologist were compared using McNemar's test. All statistical analyses were performed using SPSS (IBM® SPSS® Statistics 22; SPSS® Inc., Chicago IL). $p < 0.05$ was considered statistically significant.

3. Results

53 patients underwent MRI-examination with extracellular-fluid contrast agent, 43 patients with hepatobiliary-specific contrast agent and 12 patients with extracellular-fluid contrast agent in combination with a reticuloendothelial-specific contrast agent at a dose specified by the manufacturer (Table 1). MRI phases with reticuloendothelial-specific contrast agent were not included into TA. 43 patients had more than one lesion, the presence of satellite lesion was evaluated in conventional reading but were not used for TA.

We received histopathological results from the local pathologist of each center with the diagnosis of HCC, HA or FNH as well as the confirmation of non-cirrhotic surrounding liver parenchyma. No results of lesion sub-classifications were gathered.

For TA-features ICC between the readers showed good to excellent agreement for the arterial (0.68−0.99, median 0.96), portal-venous (0.73−0.99, median 0.92), and hepatobiliary phase images (0.64−0.98, median 0.92). Fair to excellent agreement was observed for the native fs-T1w images (0.51−0.99, median 0.95) as well as for the T2w images (0.51−0.99, median 0.92). Therefore, the data of TA Reader 1 only was used for further analysis.

ROI definition was not possible in 10 out of 108 patients for the arterial phase images, 8 in the portal-venous phase images, 9 in the hepatobiliary phase images, as well as 9 in the native fs-T1w and 7 in the T2w images due to a missing MR sequence, non-definable lesion, missing fat saturation or insufficient image quality. A flow-chart depicting the formation of the final study cohort can be found in Fig. 3.

55 patients had histopathological confirmed HCC, 24 HA and 29 FNH. In the arterial phase 53 of 97 (55%) patients had an identifiable liver lesion histopathologically confirmed as HCC, 53 of 99 (54%) in the portal-venous and 54 of 98 (55%) in the hepatobiliary phase as well as 52 of 98 (53%) in the native fs-T1w and 53 of 100 (53%) in the T2w images.

Multiple TA-features showed statistically significant differences between the HCC group and the benign liver lesion group for almost all used MRI sequences. The majority of TA-features with statistically significant differences between HCCs and benign lesions were found when arterial phase images were assessed ($n = 5$). These TA-features included skewness ($p = 0.018$) as a gray-level histogram feature and LGRE ($p = 0.001$), SRLGE ($p = 0.001$), SRHGE ($p = 0.021$) and LRLGE ($p =$

https://doi.org/10.1016/j.heliyon.2018.e00987

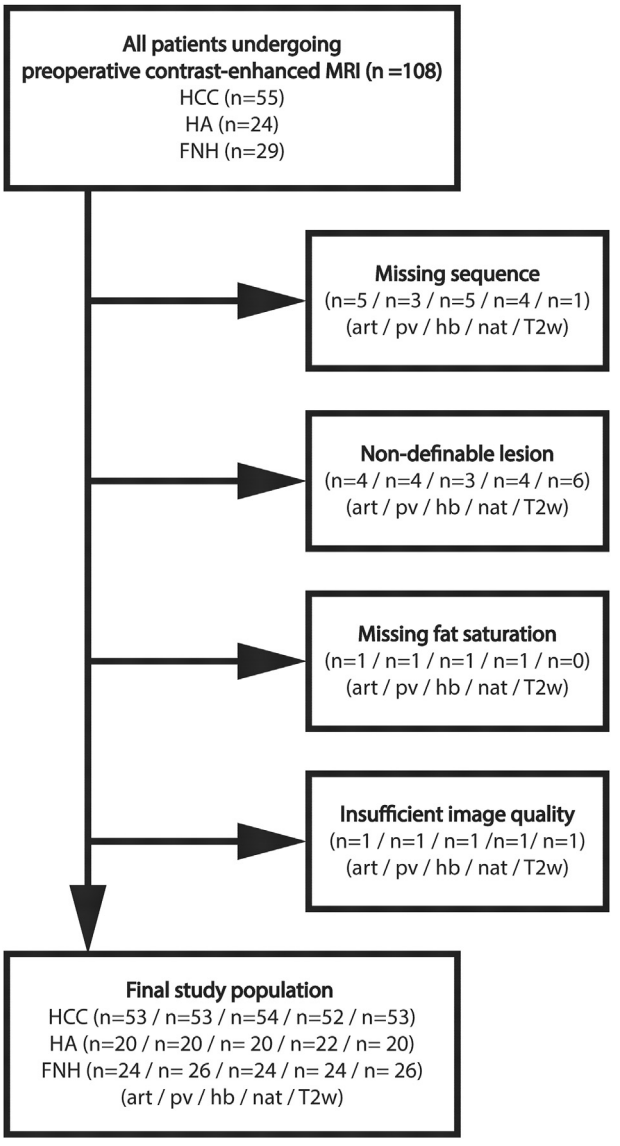

Fig. 3. Flow chart depicting the formation of the final study cohort. Abbreviations: T1-weighted arterial phase (art); T1-weighted portal-venous phase (pv); T1-weighted hepatobiliary phase (hb); T1-weighted native sequence (nat); T2-weighted sequence (T2w).

0.001) as run-length matrix features. Two TA-features with statistically significant differences between the groups were found in the portal-venous phase images (LGRE $p = 0.028$; SRLGE $p = 0.038$) and one in the native fs-T1w images (skewness $p = 0.009$). No statistically significant differences could be found when TA-features parameters in the T2w-images and in the hepatobiliary-phase images were assessed. Of note, although we found significant differences of some image features, there were also areas of overlap of these imaging features in HCCs and benign liver lesions. Box-plots of TA-features with significant differences between benign lesions and HCC for each patient are illustrated in Fig. 4.

https://doi.org/10.1016/j.heliyon.2018.e00987

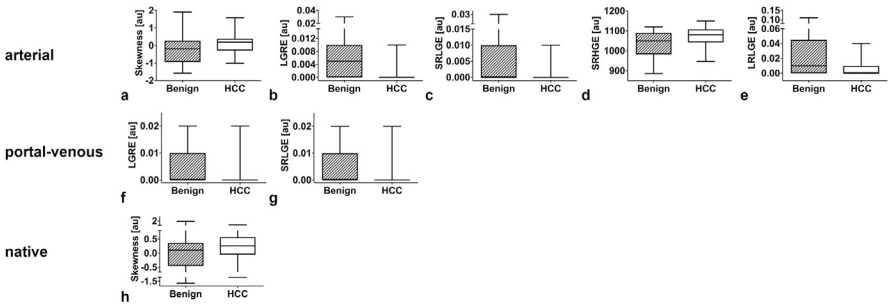

Fig. 4. Box-plots for TA-features with significant differences between benign liver lesions and HCC. Upper line: T1-weighted arterial phase; Skewness (a), LGRE (b), SRLGE (c), SRHGE (d), LRLGE (e). Middle line: T1-weighted portal-venous phase; LGRE (f), SRLGE (g). Lower line: T1-weighted native sequence; Skewness (h). Abbreviations: LGRE (low gray-level run emphasis); SRLGE (short-run low gray-level emphasis); SRHGE (short-run high gray-level emphasis); LRLGE (long-run low gray-level emphasis).

The final model obtained by binary logistic regression analysis comprised of 13 TA-features for the arterial phase images, including skewness, contrast, correlation, energy, homogeneity, entropy, LRE, GLN, RLN, LGRE, HGRE, SRLGE and LRLGE. 82 of 97 (84.5%) lesions were correctly diagnosed as HCC or benign lesions with this model. In the portal-venous phase images the resulting final model correctly diagnosed 66 of 99 lesions (66.7%), including six TA-features (kurtosis, contrast, correlation, LRE, RP, LGRE), 77 of 98 lesions (78.6%) in the hepatobiliary phase images, including eight TA-features (homogeneity, SRE, LRE, GLN, RLN, RP, HGRE, LRHGE), 67 of 98 lesions (68.4%) in the native fs-T1w images, including two TA-features (contrast, SRLGE), and 66 of 99 lesions (66.7%) including five TA-features (contrast, correlation, homogeneity, HGRE, SRHGE) in the T2w images. These results, including diagnostic accuracy, sensitivity and specificity are summarized in Table 2. The respective contingency tables are provided in Table 3.

ROC analysis yielded an AUC of 0.92 (95% confidence interval 0.85−0.98) for the arterial phase, 0.73 (95% confidence interval 0.63−0.83) for the portal-venous phase, 0.81 (95% confidence interval 0.72−0.90) for the hepatobiliary phase, 0.77 (95% confidence interval 0.68−0.86) for the native fs-T1w images and 0.68 (95% confidence interval 0.58−0.79) for the T2w images. All resulting ROC-curves are presented in Fig. 5.

Interreader agreement for conventional reading was fair with a kappa value of 0.33. 84 of 107 (78.8%) lesions were correctly diagnosed by MR Reader 1 and 67 of 107 lesions (62.6%) by MR Reader 2. These results, including diagnostic accuracy, sensitivity and specificity are summarized in Table 2.

Sensitivity of the optimal binary logistic regression model derived from arterial phase images for the diagnosis of HCC versus benign liver lesions was statistically

https://doi.org/10.1016/j.heliyon.2018.e00987

Table 2. Summarized diagnostic accuracy, sensitivity and specificity for the diagnosis of HCC versus benign liver lesions with the associated TA-features of the final model obtained by binary logistic regression analysis. Fractions of absolute numbers are shown in parenthesis. *Histogram TA-features, †GLCM-TA-features, ‡GLRLM-TA-features.

	fs-T1w native	**Arterial**	**Portal-venous**	**Hepatobilary**	**T2w**	**MR Reader 1**	**MR Reader 2**
Diagnostic accuracy [%]	68.4 (67/98)	84.5 (82/97)	66.7 (66/99)	78.6 (77/98)	66.7 (66/99)	78.8 (84/107)	62.6 (67/107)
Sensitivity [%]	78.8 (41/52) 95% CI 67.7−89.9	84.9 (45/53) 95% CI 75.3−94.5	83.0 (44/53) 95% CI 72.9−93.1	81.5 (44/54) 95% CI 71.1−91.8	79.2 (42/53) 95% CI 68.3−90.2	63.6 (35/55)	40.0 (22/55)
Specificity [%]	56.5 (26/46) 95% CI 42.2−70.8	84.1 (37/44) 95% CI 73.3−94.9	47.8 (22/46) 95% CI 33.4−62.3	75.0 (33/44) 95% CI 62.2−90.6	52.2 (24/46) 95% CI 37.7−66.6	94.2 (49/52)	86.5 (45/52)
Number of TA-features	2	13	6	8	5		
TA-features	contrast†	skewness*	kurtosis*	homogeneity†	contrast†		
	SRLGE‡	entropy†	contrast†	SRE‡	correlation†		
		contrast †	correlation†	LRE‡	homogeneity†		
		correlation†	LRE‡	GLN‡	HGRE‡		
		energy †	RP‡	RLN‡	SRHGE‡		
		homogeneity†	LGRE‡	RP‡			
		LRE‡		HGRE‡			
		GLN‡		LRHGE‡			
		RLN‡					
		LGRE‡					
		HGRE‡					
		SRLGE‡					
		LRLGE‡					

https://doi.org/10.1016/j.heliyon.2018.e00987

Table 3. Contingency table for all assessed MRI sequences comparing results of TA using the final regression model with the histopathological confirmed diagnoses.

MRI sequence			Histopathology	
			HCC	benign liver lesion
fs-T1w native	TA logistic regression model	HCC	41	20
		benign liver lesion	11	26
arterial	TA logistic regression model	HCC	45	7
		benign liver lesion	8	37
portal-venous	TA logistic regression model	HCC	44	24
		benign liver lesion	9	22
hepatobiliary	TA logistic regression model	HCC	44	11
		benign liver lesion	10	33
T2w	TA logistic regression model	HCC	42	22
		benign liver lesion	11	24

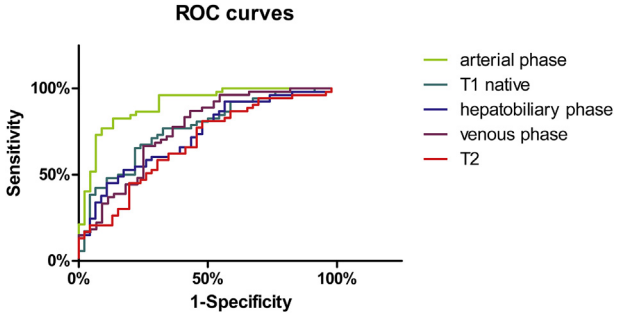

Fig. 5. ROC-curves of the final model obtained by binary logistic regression analysis for the different assessed MR images. Resulting AUC was 0.92 for the arterial phase, 0.73 for the portal-venous phase, 0.81 for the hepatobiliary phase images, 0.77 for the native fs-T1w, and 0.68 for the T2w images.

significant higher than sensitivity of MR Reader 1 ($p = 0.027$), while no statistically significant difference could be observed between the respective specificities ($p = 0.289$).

An example of misclassification of both MR readers and correct classification by TA is shown in Fig. 6.

4. Discussion

In the present study we could show, that 2D-TA is a feasible method to distinguish malignant from benign hepatocellular tumors in the non-cirrhotic liver. Most promising results were obtained when assessing arterial phase images, where the most statistically differing TA-features (including gray-level histogram as well as run-length matrix features) between HCCs and benign hepatocellular tumors as well as the

https://doi.org/10.1016/j.heliyon.2018.e00987

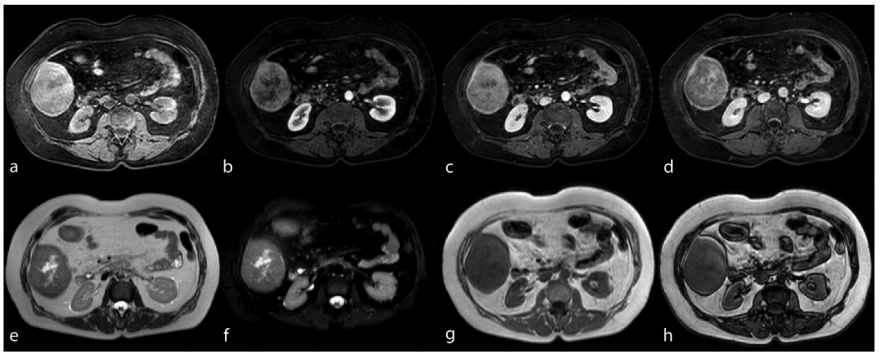

Fig. 6. Axial MR-images of a hepatocellular carcinoma in liver segment VI in a 64-year-old female patient. Upper row from left to right: native fs-T1w image (a), arterial phase (b), portal-venous phase (c) and hepatobiliary phase (d). Lower row from left to right: T2w image (e), fs-T2w image (f), in phase (g) and opposed phase (h). This lesion presents hypointense in native T1w and hyperintense in T2w and fs-T2w images. Furthermore, a T2w hyperintense central scar with increased contrast-enhancement in the hepatobiliary phase as well as slightly increased contrast-enhancing in the arterial phase compared with the surrounding liver parenchyma is seen. There was no significant change in signal intensity from the in- to the opposed-phase. Both MR readers misclassified this hepatocellular carcinoma as a focal nodular hyperplasia and hepatic adenoma, respectively, whereas texture analysis classified it correctly.

highest sensitivity, specificity and diagnostic accuracy for the correct classification of HCC were observed. In comparison to conventional reading the derived binary logistic regression model for TA-features of arterial phase images showed a statistically significant increased sensitivity while no statistical differences in specificity could be found.

Current American Association for the Study of Liver Disease (AASLD) guidelines (which were partly adopted by the European Association for the Study of the Liver (EASL)) state that HCC can be diagnosed by dynamic contrast-media (CM) enhanced MRI showing arterial CM uptake followed by washout of CM in the venous delayed phases for tumors larger than 1 cm in cirrhotic patients or patients with chronic hepatitis B [29, 30]. These features as well as the presence or absence of a pseudocapsule also play a major role in the liver imaging reporting and data system (LIRADS), which was introduced by the American College of Radiology (ACR) to standardize reporting and diagnosis of HCC in patients at high risk [31]. However, all these features remain qualitative and therefore are prone to subjective misinterpretation. TA on the other hand provides objective quantitative measures and therefore − besides the definition of a ROI − lacks this subjective component. This behavior was confirmed in our study showing a substantially higher interreader agreement for TA than for conventional reading.

MRI specific imaging features of HCC should only be applied in patients with cirrhosis or patients with chronic hepatitis B who may not have developed cirrhosis yet [29]. Although cirrhosis is the strongest predisposing factor for HCC the annual incidence of HCC in the non-cirrhotic liver is as high as 0.4% [32]. Still there are no

https://doi.org/10.1016/j.heliyon.2018.e00987

general guidelines for diagnosis of HCC in the non-cirrhotic patient. Therefore, LIR-ADS and EASL imaging criteria are commonly used for the classification of lesions in a non-cirrhotic liver as there are no systematic alternatives at the moment. Furthermore, Lin et.al [9] showed a lower sensitivity (78.9 % for CT and 65.0% for MRI) for the diagnosis of HCC in non-cirrhotic patients when compared to cirrhotic patients (85.3% for CT and 80.0% for MRI) and to our knowledge no study has assessed specificity in the non-cirrhotic patient yet.

While several TA-features showed statistically significant differences between benign liver lesions and HCC a significant overlap exists. This overlap limits the use of single TA-features for the correct classification of liver lesions even if the most appropriate MR sequence was used. Models using a combination of TA-features may provide a better approach to discriminate benign from malignant lesions. Indeed, using the optimal logistic regression model of TA-features we found a sensitivity of 84.9% and a specificity of 84.1% for the correct distinction of HCC from resected (and therefore most likely atypical) benign liver lesions, almost reaching the performance of MRI in patients with chronic liver disease (mainly cirrhosis, sensitivity 88%, specificity 94% [8]) and outperforming the diagnostic accuracy of conventional reading in the present study.

During hepatocarcinogenesis from a dysplastic nodule over early HCC and well-differentiated HCC to poor-differentiated HCC a typical shift from a portal vein dominated vascular supply to an arterial dominated vascular supply of the lesion is usually observed. When evaluating the assessed image sequences, we found the most promising results for the arterial phase images to distinguish HCC from benign liver lesions, while the accuracy for the portal-venous and hepatobiliary phase was worse. The above described transformation of the vascular supply during the stepwise development of HCC as well as the formation of leaky vessels in HCCs might be a possible explanation for this observation. The relative lack of differences of TA-features between HCC and HA as well as atypical FNH in the portal-venous and hepatobiliary phase images might be explained with the known similar behavior of HCC and HA in those phases due to a similar drainage pattern and commonly missing functional hepatocytes in these lesions. The poor performance for TA of the T2w images, however, might be explained with the heterogeneous data-set as both fat-saturated and non-fat-saturated T2w images were part of the data.

The following study limitations must be taken into account. First, MR-studies were acquired at different MR-scanners using locally optimized protocols and different contrast agents. This might have added to the observed variability and decreased measured sensitivity, specificity as well as diagnostic accuracy and might has also affected the diagnostic performance of TA. However, this setup reflects the current status of liver imaging at different centers and even in this setting significant differences could be observed. The potential impact of sequence parameters and image

https://doi.org/10.1016/j.heliyon.2018.e00987

quality on TA-features was not part of this study and has to be evaluated in further studies. Second, additional sequences such as diffusion weighted imaging sequences might have improved the results of conventional reading and TA. Third, the obtained results are only valid for the used acquisition parameters and cannot be generalized for different MR-image acquisitions as these might have an influence on the derived TA-features. Fourth, a selection bias of the included lesions might be present as only resected liver lesions were included. Furthermore, due to the exploratory nature of the present study and the main goal to identify potentially diagnostic TA features, the derived binary logistic regression models were not rigorously corrected for multiple comparisons. Consecutively these results need to be validated in further future studies in a prospective manner.

In conclusion, we could show that 2D-texture-analysis of MR images is a feasible objective method that may help to distinguish malignant from benign hepatocellular tumors. The most promising results were found in TA features in the arterial phase images.

Declarations

Author contribution statement

Daniel Stocker, Moritz Wurnig: Conceived and designed the experiments; Analyzed and interpreted the data; Contributed reagents, materials, analysis tools or data; Wrote the paper.

Matthias W. Wagner, Herman Marquez Masquiaran: Analyzed and interpreted the data.

Dimitri Raptis: Performed the experiments; Contributed reagents, materials, analysis tools or data.

Pierre-Alain Clavien: Performed the experiments; Contributed reagents, materials, analysis tools or data.

Andreas Boss: Contributed reagents, materials, analysis tools or data; Wrote the paper.

Michael Fischer: Conceived and designed the experiments; Performed the experiments.

Funding statement

The work of Matthias W. Wagner was supported by the Swiss Cancer League (KFS 3769-08-2015).

https://doi.org/10.1016/j.heliyon.2018.e00987

Competing interest statement

The authors declare no conflict of interest.

Additional information

The clinical trial described in this paper was registered at clinicaltrials.gov under the registration number NCT01234701.

References

[1] L.A. Torre, F. Bray, R.L. Siegel, J. Ferlay, J. Lortet-Tieulent, A. Jemal, Global cancer statistics, 2012, CA Cancer J. Clin. 65 (2) (2015) 87−108.

[2] M.C. Yu, J.M. Yuan, Environmental factors and risk for hepatocellular carcinoma, Gastroenterology 127 (5 Suppl 1) (2004) S72−S78.

[3] X. Calvet, J. Bruix, C. Bru, P. Gines, R. Vilana, M. Sole, M.C. Ayuso, M. Bruguera, J. Rodes, Natural history of hepatocellular carcinoma in Spain. Five year's experience in 249 cases, J. Hepatol. 10 (3) (1990) 311−317.

[4] P. Jepsen, M.W. Andersen, G.E. Villadsen, P. Ott, H. Vilstrup, Time-trends in incidence and prognosis of hepatocellular carcinoma in Denmark: a nationwide register-based cohort study, Liver Int. (2016).

[5] U.C. Nzeako, Z.D. Goodman, K.G. Ishak, Hepatocellular carcinoma in cirrhotic and noncirrhotic livers. A clinico-histopathologic study of 804 North American patients, Am. J. Clin. Pathol. 105 (1) (1996) 65−75.

[6] B. Shrager, G. Jibara, M. Schwartz, S. Roayaie, Resection of hepatocellular carcinoma without cirrhosis, Ann. Surg. 255 (6) (2012) 1135−1143.

[7] M. Burrel, J.M. Llovet, C. Ayuso, C. Iglesias, M. Sala, R. Miquel, T. Caralt, J.R. Ayuso, M. Sole, M. Sanchez, C. Bru, J. Bruix, G. Barcelona Clinic Liver Cancer, MRI angiography is superior to helical CT for detection of HCC prior to liver transplantation: an explant correlation, Hepatology 38 (4) (2003) 1034−1042.

[8] Y.J. Lee, J.M. Lee, J.S. Lee, H.Y. Lee, B.H. Park, Y.H. Kim, J.K. Han, B.I. Choi, Hepatocellular carcinoma: diagnostic performance of multidetector CT and MR imaging-a systematic review and meta-analysis, Radiology 275 (1) (2015) 97−109.

[9] M.T. Lin, C.L. Chen, C.C. Wang, Y.F. Cheng, H.L. Eng, J.H. Wang, K.W. Chiu, C.M. Lee, T.H. Hu, Diagnostic sensitivity of hepatocellular

https://doi.org/10.1016/j.heliyon.2018.e00987

carcinoma imaging and its application to non-cirrhotic patients, J. Gastroenterol. Hepatol. 26 (4) (2011) 745−750.

[10] C.B. Winston, L.H. Schwartz, Y. Fong, L.H. Blumgart, D.M. Panicek, Hepatocellular carcinoma: MR imaging findings in cirrhotic livers and noncirrhotic livers, Radiology 210 (1) (1999) 75−79.

[11] J.T. Campos, C.B. Sirlin, J.Y. Choi, Focal hepatic lesions in Gd-EOB-DTPA enhanced MRI: the atlas, Insights Imag. 3 (5) (2012) 451−474.

[12] M. Narita, E. Hatano, S. Arizono, A. Miyagawa-Hayashino, H. Isoda, K. Kitamura, K. Taura, K. Yasuchika, T. Nitta, I. Ikai, S. Uemoto, Expression of OATP1B3 determines uptake of Gd-EOB-DTPA in hepatocellular carcinoma, J. Gastroenterol. 44 (7) (2009) 793−798.

[13] J. Bruix, M. Reig, M. Sherman, Evidence-based diagnosis, staging, and treatment of patients with hepatocellular carcinoma, Gastroenterology (2016).

[14] D.C. Rockey, S.H. Caldwell, Z.D. Goodman, R.C. Nelson, A.D. Smith, American Association for the Study of Liver Diseases, Liver biopsy, Hepatology 49 (3) (2009) 1017−1044.

[15] M. Sherman, Pathogenesis and screening for hepatocellular carcinoma, Clin. Liver Dis. 8 (2) (2004) 419−443, viii.

[16] J.M. Llovet, J. Fuster, J. Bruix, G. Barcelona-Clinic Liver Cancer, The Barcelona approach: diagnosis, staging, and treatment of hepatocellular carcinoma, Liver Transplant. 10 (2 Suppl 1) (2004) S115−S120.

[17] D.S. Lu, N.C. Yu, S.S. Raman, P. Limanond, C. Lassman, K. Murray, M.J. Tong, R.G. Amado, R.W. Busuttil, Radiofrequency ablation of hepatocellular carcinoma: treatment success as defined by histologic examination of the explanted liver, Radiology 234 (3) (2005) 954−960.

[18] R.M. Haralick, Statistical and structural approaches to texture, P IEEE 67 (5) (1979) 786−804.

[19] A. Kassner, R.E. Thornhill, Texture analysis: a review of neurologic MR imaging applications, AJNR Am. J. Neuroradiol. 31 (5) (2010) 809−816.

[20] L.S. Hu, S. Ning, J.M. Eschbacher, N. Gaw, A.C. Dueck, K.A. Smith, P. Nakaji, J. Plasencia, S. Ranjbar, S.J. Price, N. Tran, J. Loftus, R. Jenkins, B.P. O'Neill, W. Elmquist, L.C. Baxter, F. Gao, D. Frakes, J.P. Karis, C. Zwart, K.R. Swanson, J. Sarkaria, T. Wu, J.R. Mitchell, J. Li, Multi-Parametric MRI and Texture Analysis to Visualize Spatial Histologic Heterogeneity and Tumor Extent in Glioblastoma, PLoS One 10 (11) (2015), e0141506.

https://doi.org/10.1016/j.heliyon.2018.e00987

[21] A. Wibmer, H. Hricak, T. Gondo, K. Matsumoto, H. Veeraraghavan, D. Fehr, J. Zheng, D. Goldman, C. Moskowitz, S.W. Fine, V.E. Reuter, J. Eastham, E. Sala, H.A. Vargas, Haralick texture analysis of prostate MRI: utility for differentiating non-cancerous prostate from prostate cancer and differentiating prostate cancers with different Gleason scores, Eur. Radiol. 25 (10) (2015) 2840−2850.

[22] S.A. Waugh, C.A. Purdie, L.B. Jordan, S. Vinnicombe, R.A. Lerski, P. Martin, A.M. Thompson, Magnetic resonance imaging texture analysis classification of primary breast cancer, Eur. Radiol. 26 (2) (2016) 322−330.

[23] M.E. Mayerhoefer, W. Schima, S. Trattnig, K. Pinker, V. Berger-Kulemann, A. Ba-Ssalamah, Texture-based classification of focal liver lesions on MRI at 3.0 Tesla: a feasibility study in cysts and hemangiomas, J. Magn. Reson. Imag. 32 (2) (2010) 352−359.

[24] O.F. Donati, R. Hunziker, M.A. Fischer, D.A. Raptis, S. Breitenstein, M.A. Patak, MRI for characterization of primary tumors in the non-cirrhotic liver: added value of Gd-EOB-DTPA enhanced hepatospecific phase, Eur. J. Radiol. 83 (7) (2014) 1074−1079.

[25] M.A. Fischer, D.A. Raptis, O.F. Donati, R. Hunziker, E. Schade, G.C. Sotiropoulos, J. McCall, A. Bartlett, P. Bachellier, A. Frilling, S. Breitenstein, P.A. Clavien, H. Alkadhi, M.A. Patak, MR imaging features for improved diagnosis of hepatocellular carcinoma in the non-cirrhotic liver: multi-center evaluation, Eur. J. Radiol. 84 (10) (2015) 1879−1887.

[26] M. Vallieres, C.R. Freeman, S.R. Skamene, I. El Naqa, A radiomics model from joint FDG-PET and MRI texture features for the prediction of lung metastases in soft-tissue sarcomas of the extremities, Phys. Med. Biol. 60 (14) (2015) 5471−5496.

[27] X. Wei, Gray Level Run Length Matrix Toolbox v1.0, 2007, 2016, http://www.mathworks.com/matlabcentral/fileexchange/download.do?objectId=17482&fn=RunLengthMatrixToolboxver1.0&fe=.zip&cid=1101680.

[28] R.M. Haralick, K. Shanmugam, I.H. Dinstein, Textural features for image classification, systems, man and cybernetics, IEEE Trans. (6) (1973) 610−621.

[29] J. Bruix, M. Sherman, American Association For the Study of Liver Diseases, Management of hepatocellular carcinoma: an update, Hepatology 53 (3) (2011) 1020−1022.

[30] European Association For The Study Of The Liver, European Organisation For Research Treatment Of Cancer, EASL-EORTC clinical practice

https://doi.org/10.1016/j.heliyon.2018.e00987

guidelines: management of hepatocellular carcinoma, J. Hepatol. 56 (4) (2012) 908−943.

[31] R.M. Haralick, S.R. Sternberg, X. Zhuang, Image analysis using mathematical morphology, IEEE Trans. Pattern Anal. Mach. Intell. 9 (4) (1987) 532−550.

[32] J.M. Llovet, A. Burroughs, J. Bruix, Hepatocellular carcinoma, Lancet 362 (9399) (2003) 1907−1917.

https://doi.org/10.1016/j.heliyon.2018.e00987